

Infrared optical properties of Pr_2CuO_4 : hint of a weak structural transition

C.C. Homes*

Department of Physics, Brookhaven National Laboratory, Upton, NY 11973

P. Fournier[†] and R.L. Greene

Center for Superconductivity Research, Department of Physics and Astronomy, University of Maryland, College Park, MD 20742

(May 20, 2019)

The temperature dependence of the reflectance of a Pr_2CuO_4 single crystal has been measured for light polarized in the a - b plane over a wide frequency range, and the optical properties determined from a Kramers-Kronig analysis. Above ≈ 250 K, the low frequency reflectance increases quickly with temperature; $\sigma_{dc} \approx \sigma_1(\omega \rightarrow 0)$ follows the functional form $e^{-E_a/k_B T}$, where $E_a \approx 0.2$ eV, which is much less than the inferred optical gap of ≈ 1.2 eV. The proximity of E_a to the phonon frequencies suggests that the *dc* transport in this material is due to thermally-activated hopping. The four infrared-active E_u modes dominate the infrared optical properties. Below ≈ 200 K, a striking new feature appears near the low-frequency E_u mode, and there is additional new fine structure at high frequency. It is proposed that the new mode and fine structure are the result of a weak structural distortion, induced by a magnetic transition, resulting in the reduction of the Brillouin zone and the activation of zone-boundary modes.

PACS: 74.25.Kc, 74.25.Gz, 74.72.Jt

I. INTRODUCTION

Within the family of high-temperature cuprate superconductors, the Ce-doped series $R_{2-x}\text{Ce}_x\text{CuO}_{4-\delta}$, where $R=\text{Nd, Sm, Eu, Gd, etc.}$, are the only materials which appear to be electron doped.¹ The region of superconductivity in the electron-doped materials is quite narrow ($x \approx 0.14 - 0.18$).² The undoped Nd_2CuO_4 and Pr_2CuO_4 are antiferromagnetic insulators, which become “bad metals” with Ce doping until the sudden onset of superconductivity at $x \approx 0.14$. There is essentially no “underdoped” region for the superconductivity, with the maximum value for the T_c ’s of 23 K and 19 K in the Nd and Pr systems, respectively, occurring at $x \approx 0.15$. At higher dopings T_c decreases rapidly vanishing above $x \approx 0.18$, and at the solubility limit ($x = 0.22$) the Nd system is metallic with no evidence of superconductivity.³ The optimally doped systems become superconducting only after oxygen reduction⁴⁻⁶ ($\delta \approx 0.01 - 0.03$), and some transport measurements suggest that both electrons and holes participate in the charge transport in the superconducting phase.^{7,8} The role played by oxygen in these materials may be more complex than in the hole-doped cuprates. It is the interesting behavior of these superconducting systems that motivates an examination of the optical properties of one of the parent compounds, Pr_2CuO_4 .

The T' structure of Pr_2CuO_4 is similar to the T structure of the hole-doped $\text{La}_{2-x}\text{Sr}_x\text{CuO}_4$; both structures are body-centered tetragonal, space group $I4/mmm$ or D_{4h}^{17} (Ref. 9). These materials consist of two-dimensional sheets of copper-oxygen layers, which define the a - b planes, with the c axis being perpendicular to the planes. The T and T' structures differ in the location of the oxy-

gen atoms between the copper-oxygen sheets. In the T structure the oxygen sits in apical sites directly above and below the copper atoms, resulting in octahedral coordination. However, in the T' structure the interplanar oxygen atoms no longer occupy the apical sites and are not chemically bonded to the copper atoms in the planes, which as a result have a square coordination.¹⁰ While the difference between the T and T' structures results in different Raman active modes, the same number of infrared active modes $3A_{2u} + 4E_u$ are expected for each.¹⁰ (The doubly degenerate E_u modes are active in the a - b planes, while the singly degenerate A_{2u} modes are active only along the c axis.)

The strong Cu-O bonding in the a - b plane of this material gives rise to two-dimensional electronic and magnetic behavior. The weak out-of-plane coupling induces long range antiferromagnetic order in the Cu spins at the relatively modest temperature of $T_{N,Cu} \approx 250 - 280$ K (Refs. 11-13), which is similar to the values of $T_{N,Cu} \approx 250 - 300$ K observed in Nd_2CuO_4 (Refs. 12,14), Eu_2CuO_4 (Ref. 15), and La_2CuO_4 (Refs. 16,17). The rare earth Pr ions carry localized $4f$ moments, which typically order at very low temperature. However, from symmetry considerations, the Pr moments should order below $T_{N,Cu}$ in this material.¹⁸ In fact, due to the significant exchange interactions between the Pr ions which are mediated through the copper-oxygen layers, there is a large Pr contribution to the susceptibility¹³ below ≈ 200 K.

The optical properties of Nd_2CuO_4 have been investigated in ceramics and single crystals at a variety of temperatures.¹⁹⁻²³ Single crystals of Pr_2CuO_4 have been investigated at room temperature²⁴⁻²⁶ and at low temperature^{10,27} (≈ 10 K), but there has been no detailed study of the temperature dependence of the op-

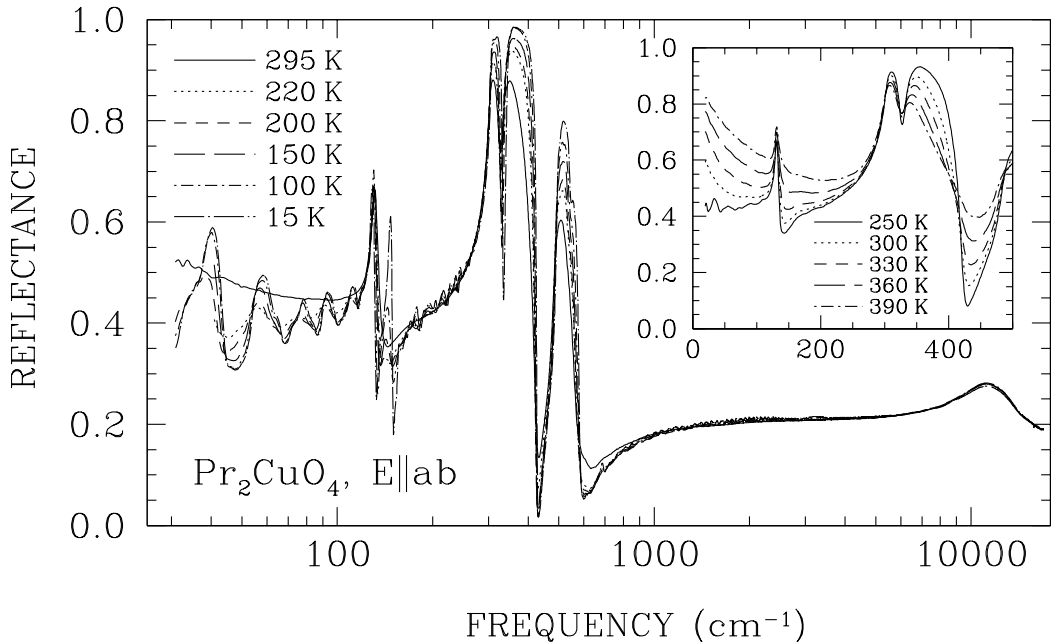


FIG. 1. (a) The reflectance of Pr_2CuO_4 for light polarized in the a - b plane for several of temperatures from ≈ 30 to over $16\,000\text{ cm}^{-1}$. The rapid appearance of the oscillatory structure at low temperature is an indication of the increasingly transparent nature of the sample. Inset: The temperature dependence of the low-frequency reflectance between 250 and 390 K, indicating an increasingly “metallic” behavior.

tical properties of this material. Furthermore, there is some disagreement in the literature with respect to the vibrational parameters of the E_u modes.

II. EXPERIMENTAL

Single crystals of Pr_2CuO_4 were grown using a CuO-based direction solidification technique.²⁸ The crystals are thin platelets $\approx 1.5\text{ mm} \times 1.5\text{ mm}$ in the a - b plane, but quite thin along the c axis ($\approx 50\text{ }\mu\text{m}$). The crystals examined had a flat, mirror-like surface which was free of flux or other residue. For the optical measurements, crystals were mounted in a cryostat on an optically-black cone. The temperature dependence of the reflectance was measured at a near-normal angle of incidence from ≈ 30 to over $16,000\text{ cm}^{-1}$ on a Bruker IFS 66v/S using an *in situ* overcoating technique, which has previously been described in detail elsewhere.²⁹ This technique is especially useful when measuring small samples, as it allows the entire face of the sample to be utilized. Above $\approx 5000\text{ cm}^{-1}$ the reflectance is assumed to be temperature independent.

The optical conductivity has been determined from a Kramers-Kronig analysis of the reflectance, for which extrapolations for $\omega \rightarrow 0, \infty$ must be supplied. At low frequency, a metallic extrapolation was used for $T \gtrsim 260\text{ K}$, $R \propto 1 - \sqrt{\omega}$; while below this temperature the reflectance was assumed to continue smoothly to ≈ 0.45

at zero frequency. At high frequency, the reflectance was assumed to be constant above the highest measured frequency point to $2 \times 10^5\text{ cm}^{-1}$, above which a free-electron ($R \propto w^{-4}$) behavior was assumed. At low temperature, the semitransparent nature of the sample has implications for the Kramers-Kronig analysis, which assumes specular reflectance from a single surface only. While the absorption due to the lattice modes assures that the reflectance in those regions is essentially that of the bulk material, the same cannot be said for the high-frequency region. The presence of multiple reflections leads to asymmetries in the line shapes and an optical conductivity less than zero. As a result, for the calculation of the low-frequency conductivity in the region of the lattice modes, the reflectance has been truncated at $\approx 3000\text{ cm}^{-1}$ and assumed to be constant only to 8000 cm^{-1} , above which a free electron approximation has been assumed. While the lineshapes in the conductivity are symmetric Lorentzians whose positions and widths do not vary greatly with different choices for the high-frequency extrapolations, the amplitudes are somewhat sensitive upon this choice.

III. RESULTS

The reflectance of Pr_2CuO_4 for light polarized in the a - b plane is shown in Fig. 1 from ≈ 30 to $16\,000\text{ cm}^{-1}$ for a variety of temperatures. The reflectance at low fre-

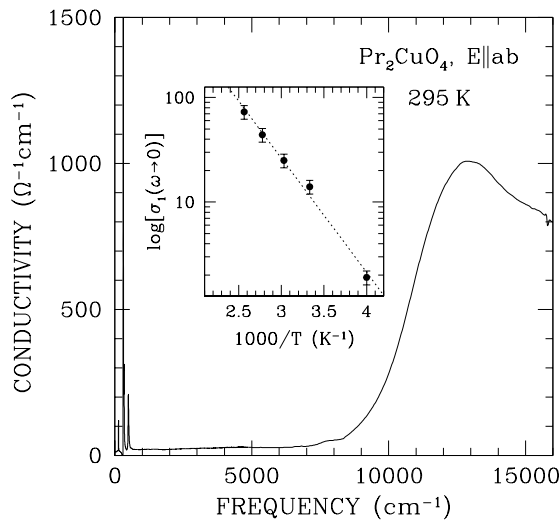


FIG. 2. The optical conductivity of Pr_2CuO_4 from ≈ 30 to $16\,000\text{ cm}^{-1}$. Inset: the log of extrapolated value for the dc conductivity vs $1/T$; the dotted line is a linear regression of the data.

quency is dominated by structure due to the normally-active infrared modes, while the reflectance at high frequency is relatively featureless, except for some structure at $\approx 11\,000\text{ cm}^{-1}$. The low-frequency vibration at $\approx 130\text{ cm}^{-1}$ is observed to be a single mode at room temperature. However, at low temperature this mode is resolved as a doublet. The low-frequency reflectance has an unusual temperature dependence; at low temperature the fringes indicate a lack of absorption due to the insulating nature of the sample, but at room temperature the fringes have vanished and the reflectance appears to be tending towards unity as $\omega \rightarrow 0$. This behavior has been examined more carefully at low frequency above room temperature in the inset Fig. 1. At 250 K, the low-frequency reflectance has the characteristics of an insulator, while at room temperature the reflectance is increasing rapidly with decreasing frequency; this trend which continues with increasing temperature until at 390 K the low frequency reflectance is over 80% and the system appears to be weakly metallic.

The optical conductivity $\sigma_1(\omega)$ calculated from a Kramers-Kronig analysis of the reflectance at 295 K is shown in Fig. 2. The low frequency conductivity is dominated by the infrared-active E_u lattice modes, but a careful examination shows a slight asymmetry in the lineshape of the strongest mode. The weak feature in observed in the reflectance at $\approx 11\,000\text{ cm}^{-1}$ signals the onset of absorption in the conductivity at about 9000 cm^{-1} , which peaks at about $12\,000\text{ cm}^{-1}$. The inset in Fig. 2 shows the extrapolated value for the log of $\sigma_{dc} \approx \sigma_1(\omega \rightarrow 0)$ vs $1/T$; the linear behavior indicates that the conductivity is strongly activated.

The optical conductivity in the region of the infrared

active modes calculated using the truncated reflectance is shown in Fig. 3. The strongest mode at $\approx 303\text{ cm}^{-1}$ is shown in the inset in Fig. 3, where unlike Fig. 2 it has a symmetric profile; this mode is characteristic of the other modes at ≈ 330 and 490 cm^{-1} in that it hardens and narrows with decreasing temperature. The reflectance of the low-frequency E_u mode is shown in Fig. 4(a) and the conductivity in Fig. 4(b). The low-frequency mode can now clearly be distinguished as fundamental at $\approx 130\text{ cm}^{-1}$. A new feature appears quickly below room temperature, gaining oscillator strength monotonically with decreasing temperature and hardening to $\approx 145\text{ cm}^{-1}$ at low temperature, as shown in the inset in Fig. 4(b). At room temperature, there is a background conductivity of $\approx 20\text{ }\Omega^{-1}\text{cm}^{-1}$ over most of the observed frequency range, which is thought to be due to activated carriers. This finite conductivity effectively renders the sample opaque at room temperature and above. The origin of the fringes at low temperature is attributed to interference effects due to reflections from the back of the crystal as the sample becomes increasingly transparent, as evidenced by the unphysical results $[\sigma_1(\omega) < 0]$ at low temperature.

Because of the complications introduced by the slightly transparent nature of the sample, the reflectance and the lattice modes have been fit using a self-consistent approach. The reflectance of a lamellar plate is $R = \tilde{r}_l \tilde{r}_l^*$, where \tilde{r}_l is defined as

$$\tilde{r}_l = \frac{\tilde{r} [1 - e^{i\omega 4\pi \tilde{n}d}]}{1 - r^2 e^{i\omega 4\pi \tilde{n}d}}, \quad (1)$$

where d is the sample thickness, and \tilde{r} is the Fresnel reflectance of the bulk material,

$$\tilde{r} = \frac{1 - \tilde{n}}{1 + \tilde{n}}. \quad (2)$$

The complex refractive index is $\tilde{n} = n + ik$, with $\tilde{\epsilon} = \epsilon_1 + i\epsilon_2 = \tilde{n}^2$, which allows the real and imaginary parts of the refractive index n and k to be determined

$$n = \left\{ \frac{1}{2} \left[\sqrt{\epsilon_1^2 + \epsilon_2^2} + \epsilon_1 \right] \right\}^{1/2}, \quad (3)$$

$$k = \left\{ \frac{1}{2} \left[\sqrt{\epsilon_1^2 + \epsilon_2^2} - \epsilon_1 \right] \right\}^{1/2}. \quad (4)$$

The optical properties of the bulk material are modeled using a series of Lorentzian oscillators

$$\tilde{\epsilon}(\omega) = \epsilon_\infty + \sum_j \frac{\omega_{p,j}^2}{\omega_{TO,j}^2 - \omega^2 - i\gamma_j \omega}, \quad (5)$$

where $\omega_{TO,j}$, γ_j and $\omega_{p,j}$ are the frequency, width and effective plasma frequency of the j th transverse optic (TO) vibration, and ϵ_∞ is the core contribution to the dielectric function. The dimensionless oscillator strength is

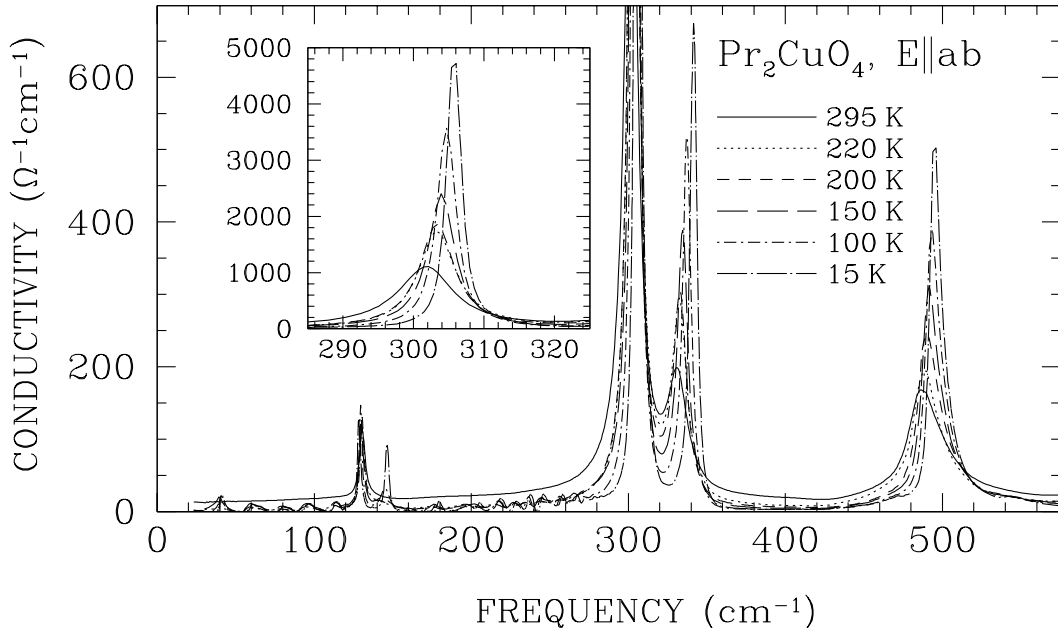


FIG. 3. The optical conductivity of Pr_2CuO_4 at low frequency for light polarized in the a - b plane for several temperatures. The optical conductivity is dominated by the four infrared-active E_u lattice modes. Note that the low-frequency mode is resolved as a doublet at low temperature. Inset: The temperature dependence of the strongest E_u vibration at $\approx 300 \text{ cm}^{-1}$.

written as $S_j = \omega_{p,j}^2/\omega_{TO,j}^2$. The optical conductivity $\tilde{\sigma}(\omega) = \sigma_1(\omega) + i\sigma_2(\omega)$ is related to the complex dielectric function by $\tilde{\sigma}(\omega) = -i\omega\tilde{\epsilon}(\omega)/4\pi$.

The phonon parameters were refined by a non-linear least-squares fit of the model for the reflectance of a thin dielectric slab to the experimental reflectance in Fig. 1. The results at 295, 200 and 15 K are listed in Table I, and a comparison of the experimental reflectance and the model results are shown in Figs. 5(a) and 5(b) at 295 and 15 K, respectively. The broad, incoherent electronic background observed at room temperature is modeled by a zero-frequency Drude term, as well as two midinfrared overdamped oscillators (Table I). The results were then compared with fits to the features in the conductivity by assuming simple linear background in the region of the lattice modes, and were found to be in good agreement. This indicates that in the region of the phonon features where the sample is opaque, the Kramers-Kronig relation yields acceptable values for the conductivity.

IV. DISCUSSION

A. Electronic properties

The peak in the optical conductivity of Pr_2CuO_4 at $\approx 12500 \text{ cm}^{-1}$ in Fig. 2 shows little or no temperature dependence, and has been observed in previous work.^{22,24,26} The location of this feature is similar to the onset of absorption in La_2CuO_4 and related materials³⁰

at $\approx 11000 \text{ cm}^{-1}$ ($\approx 1.4 \text{ eV}$). The peak is characteristic of a semiconducting band edge or a polaronic excitation. In either of these cases, the *dc* conductivity is expected to be activated and to follow the form

$$\sigma_{dc} \propto e^{-E_a/k_B T}. \quad (6)$$

The low-frequency reflectance increases quickly above room temperature, which is indicative of a “metallic” response in which the reflectance goes to unity at zero frequency. This observation is realized in the optical conductivity, where $\sigma_{dc} \approx \sigma_1(\omega \rightarrow 0)$ has a very strong temperature dependence for $T \gtrsim 300 \text{ K}$. The plot of the log of $\sigma_1(\omega \rightarrow 0)$ vs $1/T$ is shown in the inset in Fig. 2, and is described quite well by Eq. (6); a linear regression yields $E_a \approx 1750 \pm 200 \text{ cm}^{-1}$. An estimate of the direct optical gap may be made by extrapolating from the linear part of the leading edge conductivity in Fig. 2 to the ordinate, which gives $2\Delta \approx 9500 \text{ cm}^{-1}$. If the transport were due to the carrier pair density from thermal excitations across the gap, then $\sigma_{dc} \propto n_i \approx e^{-\Delta/k_B T}$. However, $E_a \ll \Delta$, suggesting that the *dc* transport is due to hopping between localized states within the gap.³¹ On the other hand, the optical conductivity of the nickelates, which has a similar appearance, has been fitted using a small-polaron model,^{32,33} which for $T \gg \omega/2$ produces an asymmetric Gaussian peak with a maximum at $4E_a$. This model would imply that the peak in the conductivity at high temperature should occur at $\approx 7000 \text{ cm}^{-1}$, which is much less than the observed value of $\approx 12500 \text{ cm}^{-1}$. Finally, the value of E_a is only somewhat larger than the energies of the lattice modes. Because hopping transport

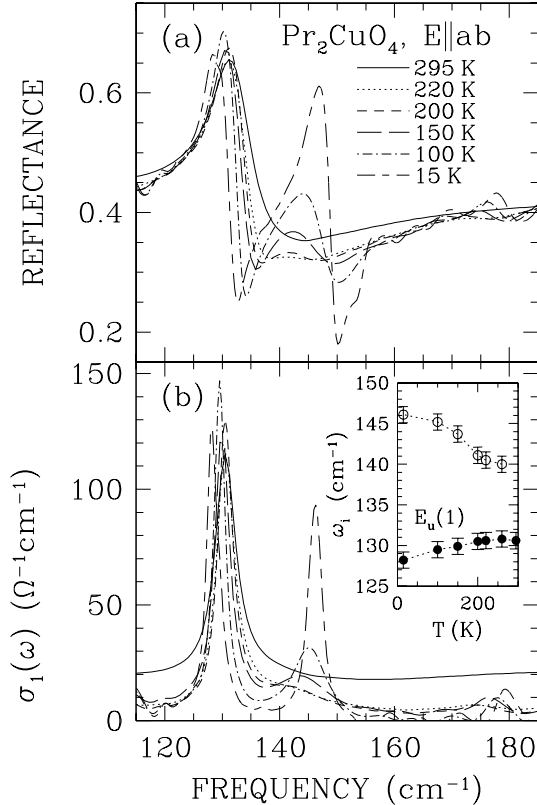


FIG. 4. (a) The reflectance of Pr_2CuO_4 for light polarized in the a - b planes in the region of the low frequency infrared-active mode. The vibration is a single mode at room temperature, but is resolved as a doublet at low temperature. (b) The optical conductivity which shows not only the appearance of a new vibrational feature, but also the rapid hardening (see inset), increase in strength and narrowing of the new mode. Inset: The temperature dependence of the fundamental mode (filled circles) and the new vibrational feature (open circles).

is assisted by optical phonons, it is likely that activated nature of σ_{dc} is due to thermally-activated hopping.

B. Vibrational properties

The infrared optical properties at room temperature are dominated by the four infrared-active E_u modes. The three high-frequency E_u modes in Fig. 3 all harden and narrow with decreasing temperature. The mode at 489 cm^{-1} at room temperature is a Cu-O in-plane stretching vibration involving mainly the oxygen atoms,¹⁰ which hardens to $\approx 495 \text{ cm}^{-1}$ at 15 K, and narrows dramatically from ≈ 25 to $\approx 8 \text{ cm}^{-1}$, as shown in Table I. The strength of this mode does not vary with temperature. The modes at ≈ 304 and $\approx 331 \text{ cm}^{-1}$ are the in-plane Cu-O bond bending modes.^{20,21} The mode

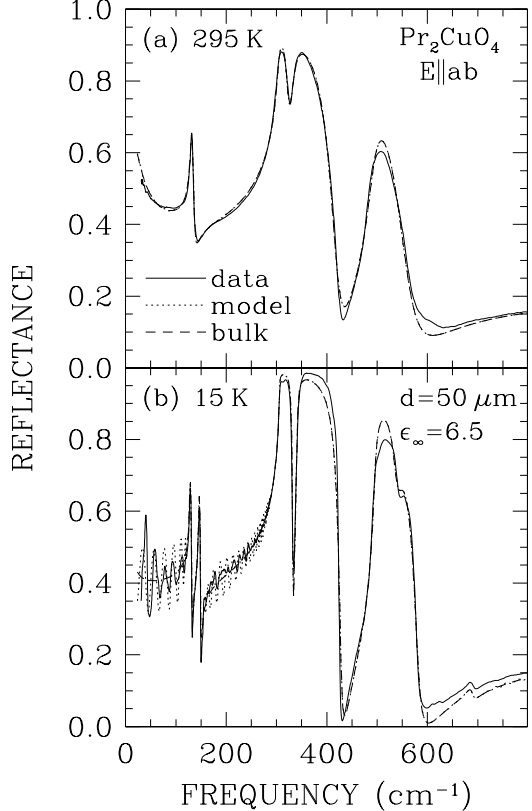


FIG. 5. (a) The reflectance in the infrared region of Pr_2CuO_4 for light polarized in the a - b plane at room temperature (solid line) and the fit to the data from Eq. (1) (dotted line) using the vibrational parameters in Table I, with $\epsilon_\infty = 6.5$ and a sample thickness of $d = 50 \mu\text{m}$. The dashed line indicates the calculated behavior of the (infinitely thick) bulk material, which is identical to that of the model, indicating the opaque nature of the sample. (b) The reflectance at 15 K (solid line) with the model fit (dotted line) using the vibrational parameters in Table I, using the same values for d and ϵ_∞ . The dashed line indicates the calculated behavior of the bulk material. The doublet structure, fringe spacing and amplitude are in good agreement with the reflectance. Note the absence of fringes in regions of strong absorption, as well as additional fine structure at high frequency.

at $\approx 304 \text{ cm}^{-1}$ hardens only slightly with decreasing temperature, and narrows from $\approx 8 \text{ cm}^{-1}$ at room temperature to 1.4 cm^{-1} at 15 K; this is the strongest E_u mode with an oscillator strength of $S \approx 7.4$. The mode at $\approx 331 \text{ cm}^{-1}$ hardens considerably to $\approx 341 \text{ cm}^{-1}$ at low temperature, and also narrows noticeably from ≈ 17 to 3.4 cm^{-1} . The slight asymmetry that is observed in the optical conductivity of the high-frequency E_u mode at $\approx 498 \text{ cm}^{-1}$ in Fig. 3 is most likely produced by the uncertainty in the high-frequency extrapolation used in the Kramers-Kronig analysis. Fits to the reflectance in Figs. 5(a) and 5(b) are exact and do not suggest a

TABLE I. The results of fitting the phonon parameters to the reflectance of Pr_2CuO_4 for light polarized in the a - b plane at 295, 200 and 15 K, using the model for a thin dielectric slab.^a A thickness of $d = 50 \mu\text{m}$ and $\epsilon_\infty = 6.5$ have been assumed. The parameters $\omega_{TO,i}$, γ_i and $\omega_{p,i}$ refer to the frequency, width and effective plasma frequency of the i th vibration. [All units are in cm^{-1} , except for the dimensionless oscillator strength $S_i = \omega_{p,i}^2/\omega_{TO,i}^2$.]

295 K				200 K				15 K			
$\omega_{TO,i}$	γ_i	$\omega_{p,i}$	(S_i)	$\omega_{TO,i}$	γ_i	$\omega_{p,i}$	(S_i)	$\omega_{TO,i}$	γ_i	$\omega_{p,i}$	(S_i)
130.7	5.3	172	(1.73)	130.4	3.3	157	(1.45)	128.2	2.7	144	(1.26)
				141.1	9.9	69	(0.24)				(0.72)
304	7.5	815	(7.18)	305	3.0	831	(7.42)	306	1.4	834	(7.43)
331	17.4	469	(2.01)	333	7.7	458	(1.89)	341	3.4	431	(1.59)
490	27.3	511	(1.08)	491	19.5	508	(1.07)	495	8.4	503	(1.03)
				541	38	112	(0.04)	542	25	108	(0.04)
				688	25	60	(0.01)	688	15	90	(0.02)

^aSeveral overdamped Lorentzian oscillators have been included in the fits to reproduce the broad, incoherent absorption attributed to thermally-activated hopping. At room temperature the Drude component (a Lorentzian centered at zero frequency) is $\gamma_0 = 420$ and $\omega_{p,0} = 620$, the parameters for the two midinfrared bands are: $\omega_1 = 1100$, $\gamma_1 = 1120$ and $\omega_{p,1} = 1270$; $\omega_2 = 4400$, $\gamma_2 = 1800$ and $\omega_{p,2} = 2200$. (All units are in cm^{-1}).

large asymmetry in this feature or others. While the observed frequencies are in good agreement with previous work,^{25,27} the linewidths are all narrower and there is only rough agreement with the reported strengths.

The most unusual feature in the reflectance spectra is striking appearance of a new low-frequency mode at low temperature, which is very close to the low frequency E_u mode, observed at $\approx 131 \text{ cm}^{-1}$ at room temperature. The new mode is not simply a peculiar artifact due to fringes in the presence of vibrational structure, as Fig. 5(b) demonstrates. While this feature has been previously observed at low temperature^{10,27} the evolution of this new mode has never been studied or explained. The low-frequency E_u mode involves the motion of most of the atoms in the unit cell, specifically the Pr atoms, the other E_u modes are primarily vibrations which involve the copper and oxygen atoms.^{20,21} The low-frequency E_u mode softens to $\approx 128 \text{ cm}^{-1}$ at low temperature, while narrowing. The new feature appears suddenly below room temperature at $\approx 140 \text{ cm}^{-1}$, as seen in Fig. 4(b) and in the inset; this mode hardens dramatically and narrows with decreasing temperature, gaining strength monotonically until it has almost the same oscillator strength as the low-frequency E_u mode (Table I). Because this feature does not appear to evolve from a strong asymmetry or shoulder in the low-frequency E_u mode, it is difficult to characterize this as a splitting of the E_u mode. Instead, it appears to be an entirely new mode.

There is additional new fine structure in the low temperature reflectance at ≈ 541 and 688 cm^{-1} . These frequencies are well above the high-frequency E_u mode at $\approx 490 \text{ cm}^{-1}$. A symmetry-breaking process would allow Raman-active A_{2u} modes as well as the longitudinal optic (LO) modes to become weakly active. However, the highest frequency for an A_{2u} mode is at $\approx 505 \text{ cm}^{-1}$ (Ref. 27), suggesting that these features are not Raman active modes. The reflectance and optical conductivity have

also been fitted using a factorized form of the dielectric function³⁴

$$\tilde{\epsilon}(\omega) = \epsilon_\infty \prod_j \frac{\omega_{LO,j}^2 - \omega^2 - i\gamma_{LO,j}\omega}{\omega_{TO,j}^2 - \omega^2 - i\gamma_{TO,j}\omega}, \quad (7)$$

where $\omega_{LO,j}$, $\omega_{TO,j}$, $\gamma_{LO,j}$ and $\gamma_{TO,j}$ are the j th LO and TO modes, and LO and TO damping, respectively. The fit at 15 K yields values for the TO modes of 128, 146, 305, 341 and 495 cm^{-1} , which are nearly identical to those shown in Table I, and LO modes at 131, 149, 332, 430 and 588 cm^{-1} , respectively. None of the LO modes are close to the new features observed at low temperature, making it unlikely that fine structure is due to LO modes.

The new structure observed at $\approx 688 \text{ cm}^{-1}$ at low temperature is similar in frequency to structure that has been observed the reflectance in other electron-doped ceramic materials³⁵ at $\approx 690 \text{ cm}^{-1}$. A number of weak features are also seen below the Néel transition in CuO, including a mode at $\approx 690 \text{ cm}^{-1}$, which has been attributed to the activation of a zone-boundary mode due to the reduction of the Brillouin zone resulting from the magnetic order.^{36,37} The induced ordering of the Pr moments inferred from neutron measurements¹³ almost exactly corresponds with the splitting of the appearance of the new low-frequency mode. This suggests that the ordering of the Pr moments arises near $T_{N,Cu}$ due to symmetry considerations and the strong interactions between the Pr ions. This magnetic transition appears to be responsible for a weak structural distortion (perhaps due to magentostriction), leading to a larger unit cell. This suggests that the weak fine structure observed in Pr_2CuO_4 at low temperature may also be due to the activation of zone-boundary modes due to the presence of magnetic order and the reduction of the Brillouin zone. The lattice dynamics of Nd_2CuO_4 have been calculated in detail,³⁸ and it is assumed that these results would be similar to those of Pr_2CuO_4 . The dispersion in the planes

of the E_u modes along the $\Gamma - X$ direction (Σ_1 branches), show that the low-frequency E_u mode does indeed harden slightly at the zone boundary, making it a good choice for the observed low-frequency mode. Furthermore, the two high-frequency E_u modes both show strong dispersion and harden considerably at the zone boundary, making them possible candidates for the observed fine structure at high frequency. The failure to observe additional fine structure near the other relatively strong E_u modes may be attributed to the general difficulty of resolving weak features in the presence of strong absorptions. Similar behavior might also be expected in Nd_2CuO_4 , where the Nd moments order below 37 K. In fact, a weak feature is observed in the reflectance of Nd_2CuO_4 at 10 K at $\approx 165 \text{ cm}^{-1}$, quite close to the low-frequency E_u mode,²⁰ and Kramers doublets have been reported in the Raman spectra at low temperature³⁹ which have been attributed to the removal of degeneracy by the Nd-Cu exchange interaction.⁴⁰ However, the temperature dependence of this feature has not been studied, so it may not be related to the ordering of the Nd moments.

V. CONCLUSIONS

The strong temperature dependence of the low-frequency reflectance above ≈ 250 K results in a $\sigma_{dc} \approx \sigma_1(\omega \rightarrow 0)$ which is exponential with temperature, following the functional form $\sigma_{dc} \propto e^{-E_a/k_B T}$, where $E_a \approx 0.2 \text{ eV}$. The transport gap E_a is only slightly larger than the phonon frequencies, but much less than the inferred optical gap $2\Delta \approx 1.2 \text{ eV}$, suggesting that the transport in this material is due to thermally-activated hopping.

The four infrared active E_u modes have been observed and detailed vibrational parameters for these modes have been determined. A prominent feature close to the low-frequency E_u mode develops at low temperature, and additional fine structure is observed at high frequency; these new features appear below $T_{N,Cu}$ at roughly the same temperature at which the Pr moments are thought to order (≈ 200 K), suggesting that the magnetic transition may result in a weak structural distortion, leading to a larger unit cell and the reduction of the Brillouin zone; as a result both the prominent low-frequency mode and the additional fine structure observed at low temperature may be due to the activation of zone-boundary modes.

ACKNOWLEDGMENTS

We would like to thank D.N. Basov, V.J. Emery, A. Moodenbaugh, J.L. Musfeldt, M. Stronquin, T. Timusk, and J.M. Tranquada for many helpful discussions. This work was supported by the Department of Energy under contract number DE-AC02-98CH10886; work in Maryland is supported by the NSF Condensed Matter Physics Division under grant No. DMR 9732736.

Research undertaken at NSLS was supported by the U.S. DOE, Division of Materials and Chemical Sciences.

* Electronic address: homes@bnl.gov

[†] Present address: Département de Physique, Université de Sherbrooke, Sherbrooke, Québec, J1K 2R1 Canada.

- ¹ Y. Tokura, and S. Uchida, *Nature (London)* **377**, 345 (1989); H. Takagi, S. Uchida, and Y. Tokura, *Phys. Rev. Lett.* **62**, 1197 (1989).
- ² H. Takagi, Y. Tokura, and S. Uchida, *Physica C* **162-164**, 1101 (1989); S. Uchida, H. Takagi, and Y. Tokura, *Physica C* **162-164**, 1677 (1989).
- ³ S.J. Hagen, J.L. Peng, X.Y. Li, and R.L. Greene, *Phys. Rev. B* **B**, 13 606 (1991).
- ⁴ F. Izumi, Y. Matui, H. Takagi, S. Uchida, Y. Tokura, and H. Assano, *Physica C* **158**, 433 (1989).
- ⁵ P.W. Klamut, *J. Alloys Comp.* **194**, L5 (1993).
- ⁶ T. Kawashima and E. Takayama-Mouromachi, *Physica C* **219**, 389 (1994).
- ⁷ W. Jiang, S.N. Mao, X.X. Xi, X. Jiang, J.L. Peng, T. Venkatesan, C.J. Lobb, and R.L. Greene, *Phys. Rev. Lett.* **73**, 1291 (1994).
- ⁸ P. Fournier, X. Jiang, W. Jiang, S.N. Mao, T. Venkatesan, C.J. lobb and R.L. Greene, *Phys. Rev. B* **56**, 14 149 (1997).
- ⁹ H. Müller-Buschbaum and W. Wollschläger, *Z. Anorg. Allg. Chem.* **414**, 76 (1975).
- ¹⁰ M.K. Crawford, G. Burns, G.V. Chandrashekhar, F.H. Dacol, W.E. Farneth, E.M. McCarron III, and J.R. Smalley, *Phys. Rev. B* **41**, 8933 (1990).
- ¹¹ D.E. Cox, A.I. Godman, M.A. Subramanian, J. Gopalakrishnan, and A.W. Sleigh, *Phys. Rev. B* **40**, 6998 (1989).
- ¹² M. Matsuda, K. Yamada, K. Kakurai, H. Kadowaki, T.R. Thurston, Y. Endoh, Y. Hidaka, R.J. Birgeneau, M. A. Kastner, P. M. Gehring, A. H. Moudden, and G. Shirane, *Phys. Rev. B* **42**, 10 098 (1990).
- ¹³ J.W. Sumarlin, J.W. Lynn, T. Chattopadhyay, S.N. Barilo, D.I. Zhigunov, and J.L. Peng, *Phys. Rev. B* **51**, 5824 (1995).
- ¹⁴ Y. Endoh, M. Matsuda, K. Yamada, K. Kakurai, Y. Hidaka, G. Shirane, and R.J. Birgeneau, *Phys. Rev. B* **40**, 7023 (1989).
- ¹⁵ T. Chattopadhyay, J.W. Lynn, N. Rosov, T.E. Greigereit, S.N. Barilo, and D.I. Zhigunov, *Phys. Rev. B* **49**, 9944 (1994).
- ¹⁶ K. Sun, J.H. Cho, F.C. Chou, W.C. Lee, L.L. Smith, D.C. Johnston, Y. Hidaka, and T. Murakami, *Phys. Rev. B* **43** 239 (1991).
- ¹⁷ S.M. Hayden, G. Aeppli, R. Osborn, A.D. Taylor, T.G. Perring, S-W. Cheong, and Z. Fisk, *Phys. Rev. Lett.* **67**, 3622 (1991).
- ¹⁸ J.P. Hill, A. Vigliante, Doon Gibbs, J.L. Peng, and R.L. Greene, *Phys. Rev. B* **52**, 6575 (1995).
- ¹⁹ L. Degiorgi, S. Rusiecki, and P. Wachter, *Physica C* **161**, 239 (1989).
- ²⁰ E.T. Heyen, G. Kliche, W. Kress, W. König, M. Cardona,

E. Rampf, J. Prade, U. Schröder, A.D. Kulkarni, F.W. de Wette, S. Piñol, D. McK. Paul, E. Morán, and M.A. Alario-Franco, Solid State Commun. **74**, 1299 (1990).

²¹ J.-G. Zhang, X.-X. Bi, E. McRae, P.C. Eklund, B.C. Sales and M. Mostoller, Phys. Rev. B **43**, 5389 (1991).

²² S. Lupi, P. Calvani, M. Capizzi, P. Maselli, W. Sadowski, and E. Walker, Phys. Rev. B **45**, 12470 (1992).

²³ P. Calvani, M. Capizzi, S. Lupi, P. Maselli, A. Paolone, and P. Roy, Phys. Rev. B **53**, 2756 (1996).

²⁴ S.L. Cooper, G.A. Thomas, J. Orenstein, D.H. Rapkine, A.J. Millis, S.-W. Cheong, A.S. Cooper, and Z. Fisk, Phys. Rev. B **41**, 11 605 (1990).

²⁵ S. Tajima, T. Ido, S. Ishibashi, T. Itoh, H. Eisaki, Y. Mizuo, T. Arima, H. Takagi, and S. Uchida, Phys. Rev. B **43**, 10 496 (1991).

²⁶ T. Arima, Y. Tokura, and S. Uchida, Phys. Rev. B **48**, 6597 (1993).

²⁷ M.K. Crawford, G. Burns, G.V. Chandrashekhar, F.H. Daicol, W.E. Farneth, E.M. McCarron, III, and R.J. Smalley, Solid. State Commun. **73**, 507 (1990).

²⁸ J.L. Peng, Z.Y. Li, and R.L. Greene, Physica C **177**, 79 (1991).

²⁹ C.C. Homes, M. Reedyk, D. Crandles, and T. Timusk, Appl. Opt. **32**, 2972 (1993).

³⁰ J.D. Perkins, R.J. Birgeneau, J.M. Graybeal, M.A. Kastner, and D.S. Kleinbert, Phys. Rev. B **58**, 9390 (1998).

³¹ N.F. Mott and E.A. Davis, in *Electronic Processes in Non-Crystalline Materials*, (Clarendon, Oxford, 1971).

³² T. Katsufuji, T. Tanabe, T. Ishikawa, Y. Fukuda, T. Arima, and Y. Tokura, Phys. Rev. B **54**, R14 230 (1996).

³³ X.-X. Bi and P.C. Eklund, Phys. Rev. B **70**, 2615 (1993).

³⁴ J.L. Servoin, Y. Luspin, and F. Gervais, Phys. Rev. B **22**, 5501 (1980).

³⁵ S.H. Wang, Q. Song, B.P. Clayman, J.L. Peng, L. Zhang, and R.N. Shelton, Phys. Rev. Lett. **64**, 1067 (1990).

³⁶ X.K. Chen, J.C. Irwin, and J.P. Franck, Phys. Rev. B **52**, 13 130 (1995).

³⁷ A.B. Kuz'menko, D. van der Marel, P.J.M van Bentum, E.A. Tishchenko, C. Presura, and A.A. Bush, Phys. Rev. B **63**, 94303-1 (2001).

³⁸ E. Rampf, U. Schröder, F.W. de Wette, A.D. Kulkarni, and W. Kress, Phys. Rev. B **48**, 10 143 (1993).

³⁹ P. Dufour, S. Jandl, C. Thomsen, M. Cardona, B.M. Wanklyn, and C. Changkang, Phys. Rev. B **51**, 1053 (1995).

⁴⁰ S. Jandl, M. Iliev, C. Thomsen, T. Ruf, and M. Cardona, Solid State Commun. **87**, 609 (1993).